Forward imaging OCT endoscopic catheter based on MEMS lens scanning

Hyeon-Cheol Park, Cheol Song, Minseok Kang, Yong Jeong, and Ki-Hun Jeong*

Department of Bio and Brain Engineering, Korea Advanced Institute of Science and Technology (KAIST), Daejeon, South Korea
**Corresponding author: kjeong@kaist.ac.kr*

Received February 7, 2012; revised April 29, 2012; accepted May 2, 2012;
posted May 3, 2012 (Doc. ID 162663); published June 26, 2012

This Letter reports a fully packaged microelectromechanical system (MEMS) endoscopic catheter for forward imaging optical coherence tomography (OCT). Two-dimensional optical scanning of Lissajous patterns was realized by the orthogonal movement of two commercial aspherical glass lenses laterally mounted on two resonating electrostatic MEMS microstages at low operating voltages. The MEMS lens scanner was integrated on a printed circuit board and packaged with an aluminum housing, a gradient index fiber collimator, and an objective lens. A home-built spectral-domain OCT system with 60 kHz A-line acquisition rate was combined with the endoscopic MEMS catheter. Three-dimensional images of $256 \times 256 \times 995$ voxels were directly reconstructed by mapping the A-line datasets along the Lissajous patterns. The endoscopic catheter can provide a new direction for forward endoscopic OCT imaging.

OCIS codes: 170.4500, 170.2150, 170.3880.

Optical coherence tomography (OCT) is an emerging technique for optical bioimaging, particularly in acquiring *in vivo*, noninvasive, noncontact and cross-sectional information of high-scattering tissues with microscopic resolution [1,2]. In particular, spectral-domain optical coherence tomography (SD-OCT) enables the development of diverse OCT endoscopes with high-speed, real-time imaging capability [3–5]. Recently, microelectromechanical system (MEMS) technology stimulates the miniaturization of endoscopic catheter. The OCT endoscopic catheter can be divided into three major types: side imaging, circumferential imaging, and forward imaging.

The side imaging provides transverse images by scanning the laser beam perpendicular to the optical axis along the catheter by use of MEMS mirrors [4–8]. The circumferential imaging, implementing fiber—prism assembly at the proximal end, can play an important role for imaging a tubular organ such as gastrointestinal tract or vasculature by rotating the entire assembly [9–11]. However, in most clinical applications, the forward imaging serves as a surgical seek-and-treat tool, which locates the probe on a target area of interest and examines abnormal tissues. The recent developments of resonant fiber-scanning endoscopes realize the forward imaging with small size. However, the method requires rather cumbersome alignments in the lateral and longitudinal directions along an optical axis to strictly focus the backscattered light at the distal end of a fiber optic probe [12–14].

This Letter reports a fully packaged endoscopic catheter for forward OCT imaging by using the MEMS lens scanner. The lens scanner includes two commercialized aspheric glass lenses of 1 mm in diameter laterally mounted on two resonating electrostatic MEMS microstages. The orthogonal movement of two lenses allows two-dimensional (2D) optical scanning of Lissajous patterns on a target surface [15]. The endoscopic catheter consists of the MEMS lens scanner, a printed circuit board (PCB), a gradient index (GRIN) fiber collimator, an objective lens, and an aluminum housing. The outer dimension is 7 mm × 7 mm with an objective lens of 5 mm in diameter. Figure 1 shows a schematic diagram and optical images of the lens-scanning-based endoscopic MEMS catheter. The objective mount head was separately designed to readily change an objective lens for desired purposes; for example, a high numerical aperture objective for higher resolution or a lower one for deeper penetration depth.

The assembly process with precise optical alignment was conducted with the silicon fiber groove and the silicon lens holders of MEMS lens scanner. The optical axis was first determined by using a pigtailed GRIN fiber collimator and an objective lens. The objective lens was carefully positioned by monitoring the beam shape at the image plane to prevent optical aberrations from the mechanical tolerance of an aluminum housing element. The MEMS lens scanner mounted on PCB was then aligned along the optical axis, where the fiber groove reduces the rotational and longitudinal misalignments between the fiber collimator and the scanning module. Finally, two scanning lenses were laterally mounted on the silicon lens holders of MEMS microstages and self-aligned along the optical axis.

The precise alignment is very critical for MEMS lens scanner to minimize off-axis aberrations during the beam scanning. However, the fiber groove and the lens holders on a single silicon chip realize precise and compact alignments between both fiber collimator and two scanning lenses within the minimum length and tolerance. Besides, this configuration of pre-objective scanning ensures forward OCT endoscopic imaging with a long working distance.

A high-speed SD-OCT system was combined with the endoscopic MEMS catheter. Figure 2 illustrates a volumetric image reconstruction from a sequence of A-line datasets through the SD-OCT system combined with the endoscopic MEMS catheter. The SD-OCT system consists of a broadband superluminescent light-emitting diode (SLED, Exalos, $\lambda_0 = 830.9$ nm, $\Delta\lambda = 46.8$ nm, Max. Power = 4.99 mW), a 2×2 fiber coupler, and a home-built spectrometer with a volume phase holographic grating (Wasatch Photonics, 1200 lpmm), a near-IR (NIR) achromatic camera lens (Thorlabs, $f = 200$ mm), a CMOS line scan camera (Basler, spL

0146-9592/12/132673-03$15.00/0

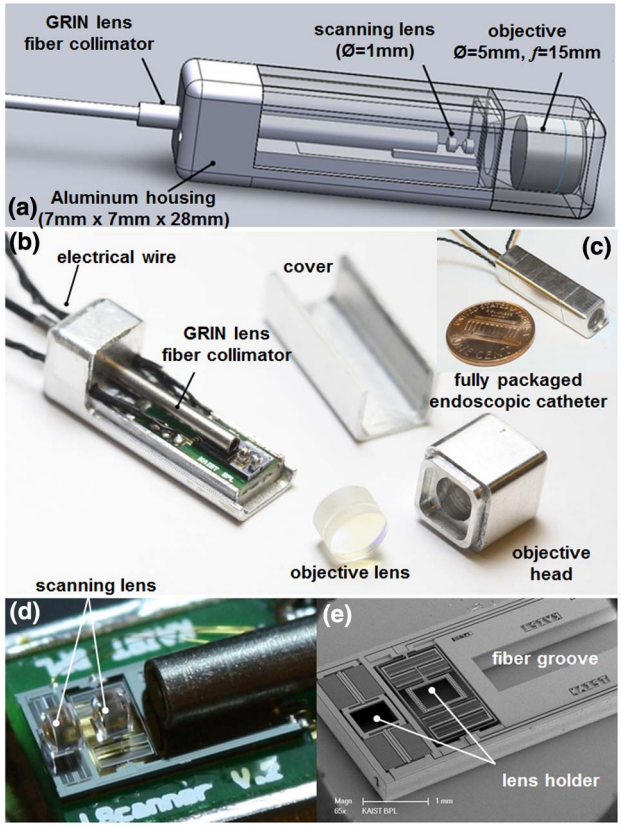

Fig. 1. (Color online) Forward imaging OCT endoscopic catheter using MEMS lens scanner: (a) schematic diagram of the endoscopic MEMS catheter, (b) catheter assembly parts, (c) fully packaged endoscopic catheter (the outer dimension of the catheter is 7 mm × 7 mm), (d) an enlarged view of the MEMS lens scanner (two scanning lenses are laterally mounted on top of the electrostatic MEMS actuators); and E, SEM image of a MEMS lens scanner. (The silicon fiber groove and the silicon lens holders assist precise optical alignment during the microassembly.)

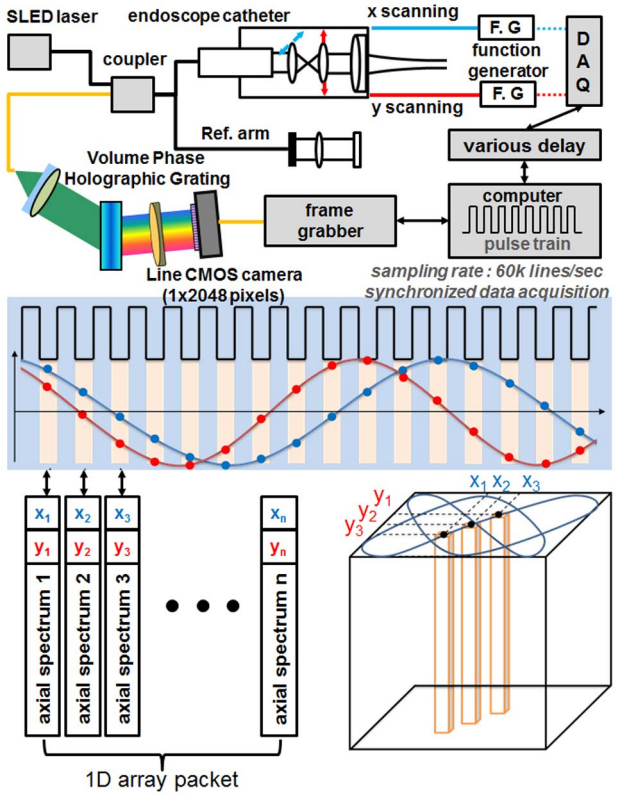

Fig. 2. (Color online) 3D SD-OCT image reconstruction sequence implementing the Lissajous-scanned endoscopic MEMS catheter. The driving signals of catheter (blue dashed line for x scanning and red line for y scanning) and the camera signals are simultaneously acquired by using the reference pulse train. The measured A-line data column set of camera signals was directly assigned at a specific location within a detection volume, which was inferred from the driving signals.

2048–2140 km) with 2048 pixel elements, and a high-speed frame grabber (National Instruments, PCIe-1429). The broadband SLED laser beam determines theoretical OCT axial resolution of 6.49 μm in air. An identical GRIN fiber collimator was implemented in both the sample arm and the reference arm to avoid a dispersion mismatch. The spectrometer resolution of 0.06 nm determines the maximum imaging depth of about 3 mm in air. While a laser beam scans along the Lissajous trajectories, the driving voltage signals of MEMS lens scanner and the measured interference spectra were simultaneously obtained from a DAQ board and a CMOS line scan camera, respectively. The individual A-line datasets were directly assigned at a specific location within a detection volume, which was inferred from the driving signals. For the precise assignment, the driving signals and camera signals were synchronized with a reference pulse train and the phase delays between the driving signals and the device motion were also compensated during the image reconstruction.

Three-dimensional (3D) OCT images were successfully obtained by combining the endoscopic MEMS catheter with a Lissajous-scanning-based 3D image reconstruction. The imaging sequence is based on a nonrepeating Lissajous pattern with a scanning trajectory that sequentially varies with each imaging frame. A similar scheme also has been utilized for miniature multiphoton microscopy [16]. The MEMS lens scanner was resonantly driven at 236 Hz in transverse direction and 293 Hz in vertical direction with low actuation voltages of DC 3 V and AC 6 V_{pp} to make nonrepeating Lissajous patterns. Each scanning frequency was adjusted within a resonance bandwidth to secure the scanning line density for a 256 × 256 image pixels, where the resolvable spot number of the MEMS lens scanner of ~100 along each axis also satisfies Nyquist criterion. The scanning frequencies still cause unsampled pixels along Lissajous trajectories due to the camera speed. However, the unsampled pixels were finally covered by averaging multiple Lissajous patterns. Figure 3 shows a volumetric OCT image of a mouse ear. In this experiment, the imaging sequence acquires 3000 A-line datasets along the nonrepeating Lissajous patterns at every 50 ms with 60 k A-line scan rate. The frame rate can be determined by the number of datasets in a single frame and the A-line scan rate, (i.e., 20 frames per second for this experiment). Each frame presents the cross-sectional images along a nonrepeating Lissajous trajectory. The 85% field of view (FOV) was also covered by repeating the Lissajous patterns for the detection time of 2.5 s. Figure 3(a) shows a partial Lissajous pattern with

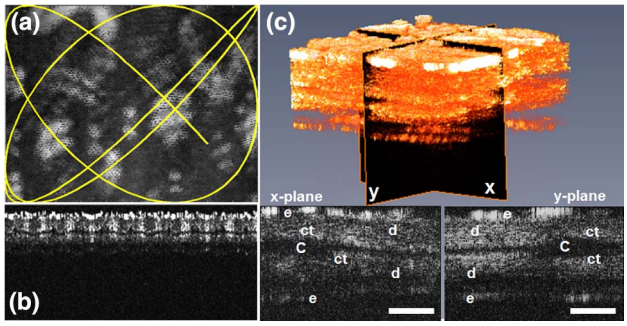

Fig. 3. (Color online) 3D SD-OCT image of a mouse ear obtained by the endoscopic catheter: e, epidermis; d, dermis; C, cartilage; and ct, connective tissue. (a) *En-face* OCT image and Lissajous trajectory (300 points). (b) Cross-sectional image along the Lissajous trajectory of 3000 points acquired within 50 ms (1 frame). (c) Reconstructed 3D SD-OCT image implementing the proposed imaging sequence. A 3D OCT image of $256 \times 256 \times 995$ voxels was reconstructed with 150 k A-line samples (50 frames). A 2D cross-sectional image of x and y axes was extracted from the 3D volumetric image (in box). Solid line indicates 500 μm.

300 measured points laid on an *en-face* OCT image. Figure 3(b) shows the cross-sectional OCT image of a single frame along the nonrepeating Lissajous trajectory. A 3D OCT image of $256 \times 256 \times 995$ ($L \times H \times D$) voxels was then reconstructed with 50 frame images by mapping the data column sets on a detection volume [Fig. 3(c)]. The transverse and axial resolutions of the sample tomogram for 2×2 mm FOV are 20 and 7.7 μm, respectively. The 2D cross-sectional images in arbitrary axes were extracted from the reconstructed 3D volumetric image as shown in the subset images of Fig. 3(c). Both OCT images show the whole layers of a mouse ear; i.e., from the surface, light layer corresponding to the epidermis followed by dermis, underlying connective tissue layer, and the dark layer corresponding to the cartilage in the middle are clearly observed. The layers are then repeated in reverse order. The imaging sequence enables direct reconstruction of a 3D volumetric image, which facilitates the selection of scanning frequencies during Lissajous scanning.

To conclude, a lens-scanning-based endoscopic MEMS catheter has been fully packaged and combined with a high-speed SD-OCT system for forward imaging. The MEMS lens scanner enables 2D optical scanning with minimum deflection of the optical axis within a spatially confined endoscopic catheter. While the additional lens mass increases mechanical quality factor and enables low voltage operation, the high quality factor may cause the motion phase delay due to external perturbations. However, the effect can be avoided by selecting the scanning frequency at semiresonance [14]. Besides, the 2D cross-sectional images were successfully obtained along the nonrepeating Lissajous trajectories and a 3D volumetric OCT image was directly reconstructed by mapping each A-line dataset on a detection volume. This imaging sequence allows the resonant operation of not only a MEMS lens scanner but also other MEMS scanners for diverse OCT microendoscopy. The current catheter has an outer dimension of 7×7 mm due to the 5 mm diameter of an objective lens, while the MEMS lens scanner is 2.7 mm in width. However, further miniaturization of the endoscopic catheter can be realized by employing advanced packaging methods with a small objective lens. The system compactness and forward viewing capability can provide a new direction for not only endoscopic OCT biopsy but also diverse *in vivo* applications such as optogenetic stimulation or 3D forward-imaging-guided laparoscopic surgery.

The authors acknowledge all staff at the Korea Advanced Institute of Science and Technology (KAIST) National Nanofab Center (NNFC) for their partial support in microfabrication. This work was supported by the National Research Foundation of Korea (NRF) and grants funded by the Korean government (MEST) (nos. 2011-0031868, 2011-0016481) and KAIST Future Systems Healthcare Project from the Ministry of Education, Science and Technology.

References

1. D. Huang, E. Swanson, C. Lin, J. Schuman, W. Stinson, W. Chang, M. Hee, T. Flotte, K. Gregory, C. Puliafito, and J. Fujimoto, Science **254**, 1178 (1991).
2. J. G. Fujimoto, M. E. Brezinski, G. J. Tearney, S. A. Boppart, B. Bouma, M. R. Hee, J. F. Southern, and E. A. Swanson, Nat. Med. **1**, 970 (1995).
3. J. Su, J. Zhang, L. Yu, and Z. Chen, Opt. Express **15**, 10390 (2007).
4. K. H. Kim, B. H. Park, G. N. Maguluri, T. W. Lee, F. J. Rogomentich, M. G. Bancu, B. E. Bouma, J. F. de Boer, and J. J. Bernstein, Opt. Express **15**, 18130 (2007).
5. W. Jung, D. T. McCormick, Y.-C. Ahn, A. Sepehr, M. Brenner, B. Wong, N. C. Tien, and Z. Chen, Opt. Lett. **32**, 3239 (2007).
6. Y. Pan, H. Xie, and G. K. Fedder, Opt. Lett. **26**, 1966 (2001).
7. A. D. Aguirre, P. R. Hertz, Y. Chen, J. G. Fujimoto, W. Piyawattanametha, L. Fan, and M. C. Wu, Opt. Express **15**, 2445 (2007).
8. J. Sun, S. Guo, L. Wu, L. Liu, S.-W. Choe, B. S. Sorg, and H. Xie, Opt. Express **18**, 12065 (2010).
9. G. J. Tearney, S. A. Boppart, B. E. Bouma, M. E. Brezinski, N. J. Weissman, J. F. Southern, and J. G. Fujimoto, Opt. Lett. **21**, 543 (1996).
10. G. J. Tearney, M. E. Brezinski, B. E. Bouma, S. A. Boppart, C. Pitris, J. F. Southern, and J. G. Fujimoto, Science **276**, 2037 (1997).
11. P. H. Tran, D. S. Mukai, M. Brenner, and Z. Chen, Opt. Lett. **29**, 1236 (2004).
12. X. Liu, M. J. Cobb, Y. Chen, M. B. Kimmey, and X. Li, Opt. Lett. **29**, 1763 (2004).
13. L. Huo, J. Xi, Y. Wu, and X. Li, Opt. Express **18**, 14375 (2010).
14. S. Moon, S.-W. Lee, M. Rubinstein, B. J. F. Wong, and Z. Chen, Opt. Express **18**, 21183 (2010).
15. H.-C. Park, C. Song, and K.-H. Jeong, Opt. Express **18**, 16133 (2010).
16. C. L. Hoy, N. J. Durr, and A. Ben-Yakar, Appl. Opt. **50**, 2376 (2011).